[American Journal of Science, Vol. 308, September, 2008, P. 843–850, DOI 10.2475/07.2008.02]

RADIOGRAPHIC IMAGING BELOW A VOLCANIC CRATER FLOOR WITH COSMIC-RAY MUONS

HIROYUKI K.M. TANAKA*,**,***,†, TOSHIYUKI NAKANO§, SATOSHI TAKAHASHI§, JUNNYA YOSHIDA§, MINORU TAKEO*, JUN OIKAWA*, TAKAO OHMINATO*, YOSUKE AOKI*, ETSURO KOYAMA*, HIROSHI TSUJI*, HIROMITSU OHSHIMA§§, TOKUMITSU MAEKAWA§§, HIDEFUMI WATANABE*, and KIMIO NIWA§

ABSTRACT. We present a novel application of cosmic-ray muon radiography to image the shallow density structure beneath Asama Volcano, Japan. We use a single detector (emulsion cloud chamber) set up in an underground vault at an elevation of 2250 m on the eastern flank of Asama, 310 m below the summit of the edifice and 1 km away from the crater. The results point to two high-density anomalies located between the original pre-2004 eruption crater floor and post-2004 eruption crater profile. A third low-density anomaly is imaged immediately below the pre-2004 eruption crater floor. The spatial extent of each density anomaly is about 100 to 200 m. To know if this method, applied to other volcanoes, would produce contrasting results, we performed the measurement in 1944 Usu lava dome. We confirmed a bulbous shape measuring approximately 300 m in diameter and narrowing downwards. The diameter of the uppermost part of the conduit is estimated at 100 ± 15 m at an elevation of 260 m a.s.l. and 50 ± 15 m at an elevation of 217 m a.s.l., demonstrating a resolution that is significantly better than that typically achieved with seismic tomography based on picks of first arrival times from earthquakes or artificial sources.

INTRODUCTION

Cosmic-ray muons arrive from angles spanning the upper hemisphere with an extremely small number of neutrino-induced upward muons. These particles are highly penetrative, and a typical horizontally-arriving cosmic ray muon with energy of 1 TeV can penetrate 2.6 km of water. Thus, cosmic-ray muon radiography can be applied to kilometer-size objects located above where a detector is placed. Cosmic-ray muon radiography is essentially the same as X-ray radiography, except penetrating muons serve in place of X-rays. In cosmic-ray muon radiography, the intensity of an image pixel is determined by the attenuation of incident muons caused by absorption in matter. This technique is completely independent of the geophysical model, and directly measures the density length (density x path length). Thus, the measurement gives us the average density $\langle\rho\rangle$ along the path lines of cosmic-ray muons through matter. The interaction cross sections can be calculated by exploiting relations in Standard Model of muon-initiated interactions which is sufficiently well known for the purpose of radiography. The inset of figure 1 shows the comparison of the zenith-angle dependence of the total muon count with the theoretically estimated angular dependence. We can see that uncertainty on the shape and amplitude of the energy spectrum of the muon source is within a few percent for different zenith angles. By measuring the muon absorption rate, we can detect a small change in $\langle \rho \rangle$ due to the existence of either lower density or higher density parts inside. The observation time is inversely proportional to the size of the detection area. For example, the time required for resolving a 3-percent change in $\langle \rho \rangle$ in a 1-km rock is two months with a 1,000-cm2

*Earthquake Research Institute (ERI), University of Tokyo, 1-1-1 Yayoi, Bunkyo, Tokyo 113-0032, Japan
**Atomic Physics Laboratory, RIKEN, 2-1 Hirosawa, Wako, Saitama 351-0198, Japan
***Physics Department, University of California, Riverside, California 92521, USA
§Physics Department, Nagoya University, Furo-cho, Chikusa, Nagoya, Aichi 464-8602, Japan
§§Usu Volcanic Observatory, Hokkaido University, Sohbetsu-cho, Usu-gun, Hokkaido 052-01, Japan
†Corresponding author email: ht@riken.jp

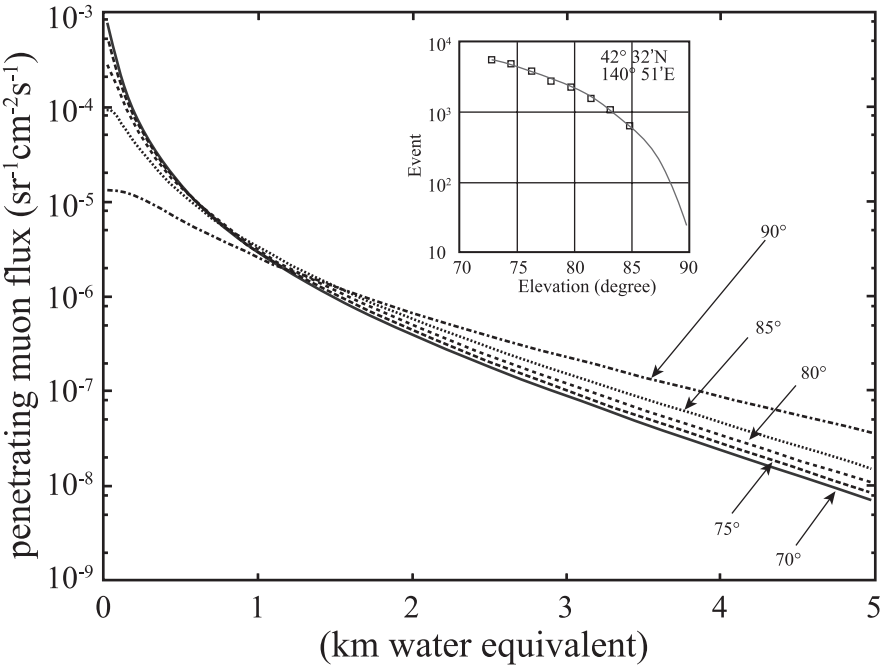

Fig. 1. Integrated flux of cosmic-ray muons at various zenith angles penetrating through a given thickness of rock with a density of 2.5 g/cm^3. The inset shows the comparison of the zenith-angle dependence of the total muon count with the theoretically estimated angular dependence at the observation site of 42°32'N, 140°51'E.

detector at solid angle intervals of 0.01 sr. Several groups have detected these changes to see inside pyramids (Alvarez and others, 1970) and volcanoes (Tanaka and others, 2003, 2005, 2007). In this paper, we present a novel application of cosmic-ray muon radiography where the image resolution is significantly higher than that typically achieved with seismic tomography based on picks of first arrival times from earthquakes or artificial sources.

COSMIC-RAY MUON RADIOGRAPHY

Radiography using the propagation of muons assumes a muon source with a well known energy spectrum for different zenith angles, a well understood muon detector, and a specific muon propagation model through matter. If the matter structure along the path line is unknown, the information from counting muon events at different arriving angles can be used to infer the matter profile. The energy spectrum of cosmic-ray muons for different zenith angles is obtained from a compilation of experimental data, and is sufficiently well known for the purpose of radiography. Thompson and others (1975) assumes that the muon parents are pions and kaons with production spectra of the form $1.8 \times 10^{-6} E^{-2.7}$ (nucleons cm^{-2} s^{-1} sr^{-1} TeV^{-1}). According to a compilation of the experimental data, the differential muon spectrum N_μ at sea level can be written as follows.

$$N_\mu(E_\mu, \theta^*)dE_\mu = 1.8 \times 10^{-6} W_\mu(E_\mu + \Delta E_\mu)^{-\gamma} \times \left(\frac{r_\pi^{\gamma-1} B_\pi \sec\theta^*}{E_\mu + \Delta E_\mu + B_\pi \sec\theta^*} + 0.36 b_r \frac{r_K^{\gamma-1} B_K \sec\theta^*}{E_\mu + \Delta E_\mu + B_K \sec\theta^*} \right) (\mathrm{cm}^{-2}\,\mathrm{s}^{-1}\,\mathrm{sr}^{-1}\,\mathrm{TeV}^{-1}), \quad (1)$$

where E_μ is the muon energy, θ* is the zenith angle, W_μ is the survival probability. The ratio of the muon momentum to the momentum of the parent pion r_π is 0.78 and the parent kaon r_K is 0.52. b_r=0.635 is the branching ratio of the $K_{\mu 2}$ decay mode. In this equation, the density length of air is L_0=1.013 kg/cm^2, with corresponding muon energy loss ΔE_μ=2.6 GeV. The survival probability is related to the average decay length L_{decay} of the muon, which is given by:

$$L_{decay} = c\,\beta\,\gamma\,\tau = 3 \cdot 10^8\,(\mathrm{m/s}) \cdot E\,(\mathrm{GeV})/m_\mu \cdot 2.2 \cdot 10^{-6}(\mathrm{s}) = 6.2 \cdot E\,(\mathrm{GeV})\ \mathrm{km}, \quad (2)$$

where γ ($=E/m_\mu$) is the Lorentz gamma factor, $c\tau$ (=660 m) is the muon decay length, and $\beta = v/c$. B_π (=90 GeV) and B_K (=442 GeV) are the decay constants of the charged pions and kaons, respectively. Equation (1) shows the behavior of the muon flux as a function of zenith angle and energy. The two terms in braces show that the contribution to the muon flux from pion and kaon decays becomes increasingly important with higher energies.

Second, the stopping power of high energy muons through matter has been studied well as has been summarized in various articles (Adair and Kasha, 1976; Particle Data Group, 1998; Groom, 2001). The energy loss of a charged particle of energy E (TeV) through matter with a certain thickness in terms of the density length of X meter water equivalent (m.w.e.) can be written as (Adair and Kasha, 1976):

$$\mathrm{d}E/\mathrm{d}X = [1.88 + 0.077 \ln (E/M_\mu) + 3.9E] \times 10^{-6}(\mathrm{TeV\ g^{-1}\ cm^2}), \quad (3)$$

Where the first two terms represent the ionization loss and the third term represents various stochastic processes, due to bremsstrahlung, direct pair production, and photonuclear interactions. Only the integrated effect leads to attenuation of flux. Because the muons interact with electrons and nucleons, the attenuation directly depends on the matter density with an extremely tiny remaining uncertainty from chemical composition. Once the density length (X) along the path line is given, the minimum energy (E_c) of the cosmic-ray muons which can penetrate through the rock is determined by equation (3). By integrating from E_c to infinity we obtain the integrated muon events $N_\mu(E_c, \theta^*)$. Inversely, for a substance with unknown X, a measurement of the muon flux $N_\mu(E_c, \theta^*)$ uniquely determines its density length. Figure 1 shows the integrated flux of cosmic-ray muons at various zenith angles penetrating through a given thickness of rock with a density of 2.5 g/cm^3. With a known energy source and known characteristics of energy absorption through matter, and well-understood detector, the "density lengths" along individual muon paths are therefore uniquely determined from a measurement of the muon flux as a function of zenith angle.

To quantify the shallow density structure below the crater floor, we use a single detector (emulsion cloud chamber; ECC) set up in an underground vault at an elevation of 2250 m on the eastern flank of Asama, 310 m below the summit of the edifice and roughly 1 km away from the crater floor (fig. 3). The detector is made of iron plates and nuclear emulsion films (Nakamura and others, 2006) and its detection area is 4,000 cm^2. The usable ranges of angles spanned by muon paths crossing the upper part of the edifice and sampled by the detector are 20 degrees in elevation and 45 degrees in azimuth. Analysis of these data yields a map of transmitted muon intensity along these paths, from which an average density can be obtained along a vertical cross section of the crater parallel to the horizontal edge of the detector. The detector elements of an emulsion film are the same as photographic films, that is micro-crystals of AgBr. When a fast charged particle passes through this layer, part of the micro-crystals on the particle trajectory becomes developable. After development, the trajectory can be recognized as a sequence of three dimensionally ordered grains.

Mt. Asama, which erupted on September 1, 2004, is one of the most active andesitic volcanoes in Japan. The summit elevation is 2560 m above sea level, and the

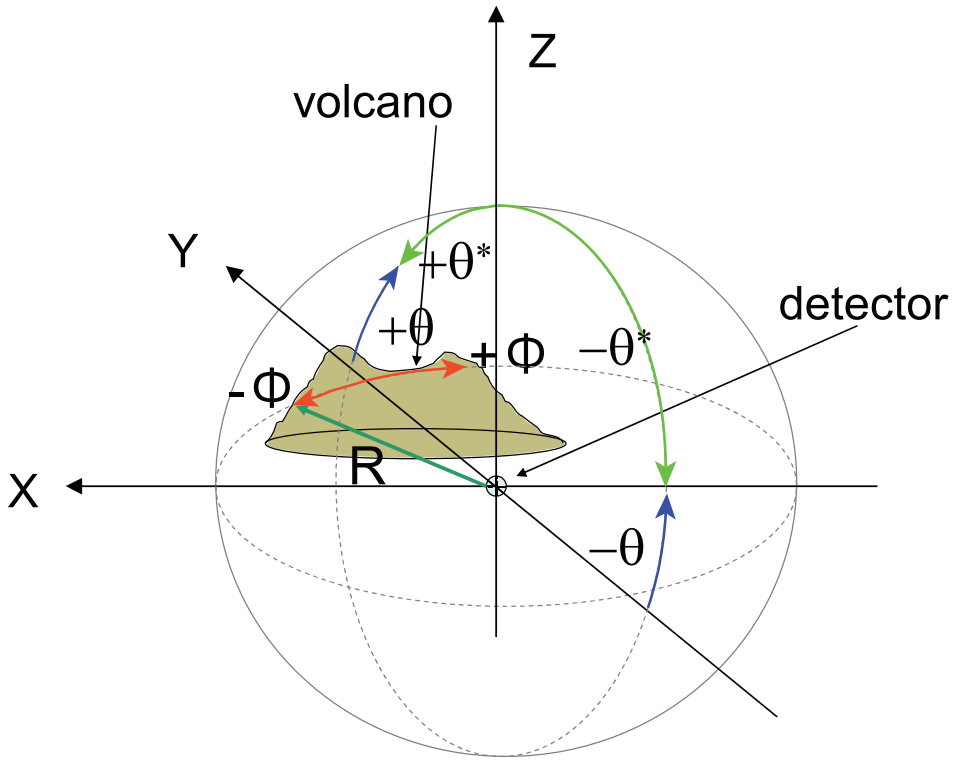

Fig. 2. Coordinate system and angles used in the relation to the detector.

size of the crater is 350 m in diameter (fig. 2). The pre-2004 eruption and post-2004 eruption crater profiles are surveyed by Urabe and others (2006). The initial investigations with the emulsion cloud chamber have been surveyed for radiography of Mt. Asama with a small detection area (700 cm^2) and its detection accuracy and performance were evaluated by imaging the external shape of the mountains and the upper most region of the main crater (Tanaka and others, 2007). The data processing methods for the ECC cosmic ray data analysis are described in detail elsewhere (Nakamura and others, 2006) and only briefly described here. Tracks from the emulsion films were digitized and read into a computer. 16 tomographic CCD (charge coupled device) images are read through a microscope in 45 micron thick emulsion layers, and tracks in these images were recorded in three dimensions by an image processor.

RESULTS AND DISCUSSIONS

In the reconstructing procedure, various muon paths are created. Because the size of the detector is much smaller than the spatial resolution of the vertex point at the target, the path of the muon can be represented by the azimuth, ϕ and elevation angle, θ with reference to the line perpendicular to the detector plane (θ, ϕ; $\theta = 90^o$-θ^*). A plot of the coordinate system and angles used in relation to the detector is shown in figure 2. The obtained histogram of the N_μ events as a function of (θ, ϕ) can be normalized by the cosmic-ray muons not passing through any substance.

We find two interesting features in the radiograph. First, the relatively strong muon-absorption region coincides with the position and the shape of the lava mound newly-created on the original pre-2004 eruption crater floor (blue dotted line in

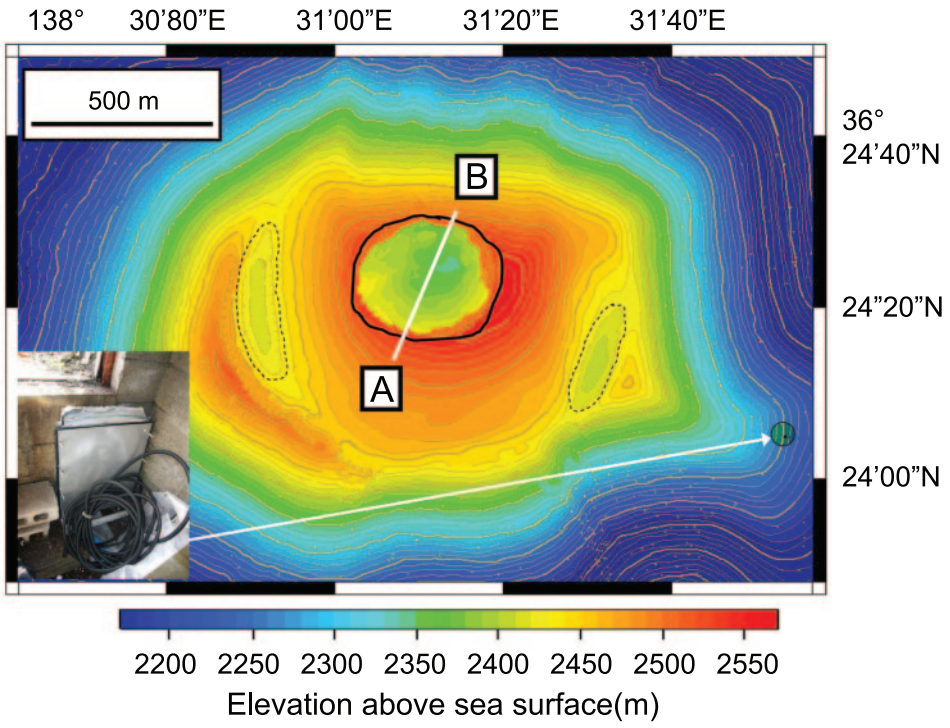

Fig. 3. Map of Mt. Asama showing the location of the cosmic-ray muon detector. Inset is the photograph showing the emulsion-cloud-chamber cosmic-ray muon detector made of iron plates and nuclear emulsion films. The white solid line A-B, parallel to the horizontal edge of the detector, indicates the top view of the vertical cross-sectional plane of the crater in figure 2. The old crater (dotted black line) of Mt. Maekake-yama has been buried with a new pyroclastic cone (Mt. Kama-yama) with a summit crater (solid black line).

fig. 3A), indicating the original crater is covered with solidified or half-solidified dense lava.

Using the conventional cosmic-ray muon absorption rate through matter, we estimated the average density of the lava mound. A particle tracking simulation was performed to compute the average density distribution. First, we defined the geometry of the target from the 1/25000 topographic map distributed by GSI (Geological Survey Institute Japan). Throughout this work default physical processes were used in GEANT4 (Agostinelli and others, 2003). In order to simulate the cosmic muon flux, each muon is treated as an individual beam that is generated in front of the detector with randomized incident angle. The muon momentum spectrum is based on the measurements of the muon flux (eq. 1) with a cut off for energies below 1 GeV. Simulation of the incident angle distribution was generated with a minimum deviation from zenith set to 60°. After the interactions, particle tracks are computed. If the particle that interacts with the detectors is a muon the zenith and azimuth angles of the muon track is written to a data file.

The average density ($\langle\rho\rangle$) mapping (fig. 4B) shows that the $\langle\rho\rangle$ along the muon path lines through the lava region is about 5 percent higher than those through the surrounding area at the same depth. Considering the ratio of the path length between the lava mound and the surrounding rock of ~0.2, and the radiographically determined surrounding density of 2.27 to 2.33 g/cm^3, we find that the bulk density of the lava mound is 2.76 to 2.84 g/cm^3. The value is typical for andesitic magma. The radiographic image indicates that the volcanic conduit is now sealed at the top by the

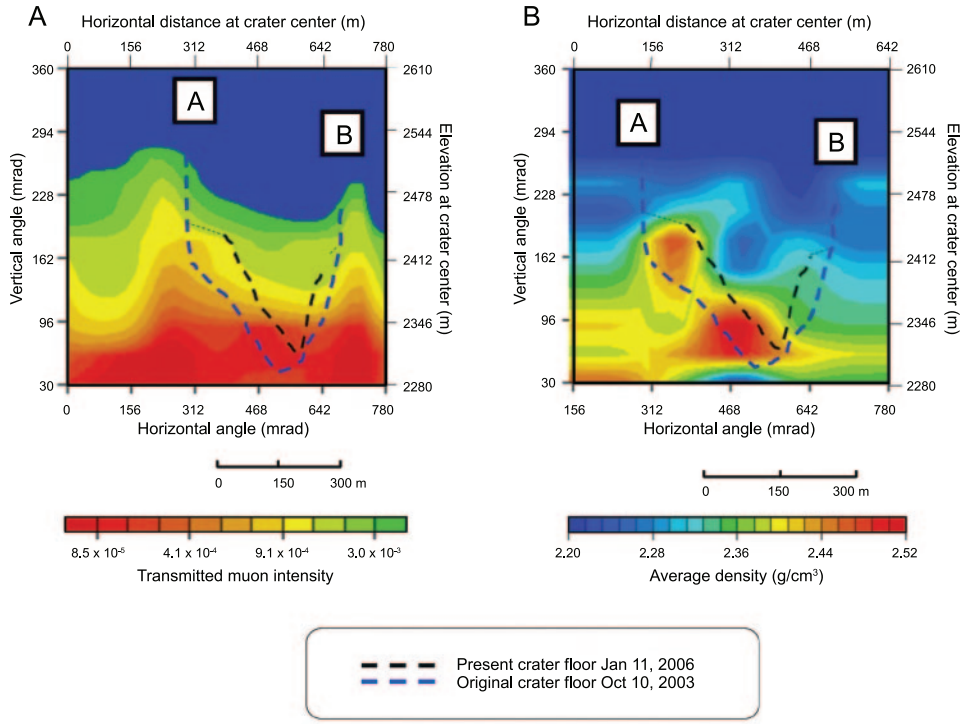

Fig. 4. (A) Radiographic image of the summit region of Mt. Asama. (B) The reconstructed average density distribution for each path line. The region above the elevation where the detector was placed is plotted. The position and the shape of the original pre-2004 eruption crater floor and post-2004 eruption crater profile are overlaid on each plot. The bottom and the left axis indicate the horizontal and vertical angles (θ, ϕ in unit of mrad) with reference to the line perpendicular to the detector plane. The top and right axis in unit of meter corresponds to the horizontal distance and the elevation at the center of the crater. Radiographic image is plotted as transmitted muon intensity.

large mass of the vent cap. Exsolved volatiles and vaporized ground water may be confined below this lava cap in the next eruption.

Second, we find the relatively weak muon-absorption region, indicating lower density below the pre-2004 eruption original crater. One possible physical process to create a low density region below the crater floor is fall-back of fragmented materials into the vent and upper conduit. This fall-back mechanism yields results consistent with the intermittent collapses of the crater floor that occurred between 22 October 2004 and 11 January 2006 (Urabe and others, 2006). After the eruption ended, the collapse of the crater floor began, presumably reflecting the fall-back. Our interpretation of the low density region is that the fall-back process created the porous magma supply path below the crater floor. The $\langle\rho\rangle$ along the muon path through this region is about 6 percent lower than that through the surrounding area at the same depth (fig. 4B). Assuming this porous region is localized in the vent area, it is explained by a conduit diameter of 150 $\pm$ 60 m (where the error corresponds to the horizontal resolution of the image which is limited to the statistics available here) with bulk density of 0.8 $\pm$ 0.2 g/cm^3. This value corresponds to a porosity of 25 to 45 percent, inferring very high permeability.

To know if this method, applied to other non-Vulcanian volcanoes, would produce contrasting results, we performed cosmic-ray muon radiography in the 1944 Usu lava dome which extruded as a parasitic cone of Usu, Hokkaido, Japan. We

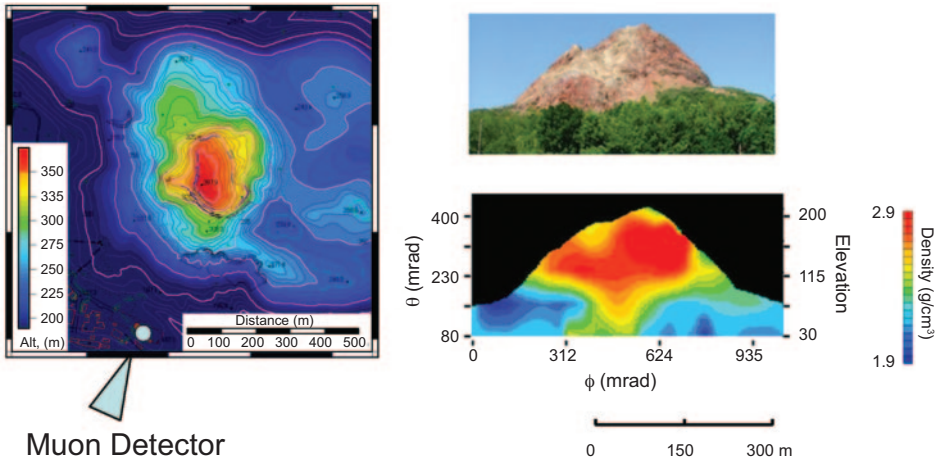

Fig. 5. Radiographic image of the conduit beneath 1944 Usu lava dome. (left) a map of the lava dome showing the location of the cosmic-ray muon detector (arrow). (right) the exterior shape of the lava dome and the average density distribution. The average density distribution is projected on the cross sectional plane that is parallel to the detector plane and includes the dome peak. The coordinate at the right side indicates elevation in m.

reconstructed the subsurface crustal density structure (right panel of fig. 5) by comparing the transmission image with the local topographic structure (left panel of fig. 5) by referring to the integrated flux of muons at various zenith angles penetrating through a given thickness. This is essentially a cross section through the dome parallel to the plane of the detector, on which the average density along all the muon paths is projected. The image is drawn with a vertical spatial resolution of ±15 m and a horizontal resolution of ±15 m. High density region can be seen beneath the dome. This region may be explained by a conduit diameter of 100 ± 15 m at an elevation of 145 mrad and of 50 ± 15 m at an elevation of 60 mrad. The measurement confirmed a bulbous shape measuring approximately 300 m in diameter and narrowing downwards. The result is consistent with a model proposed by Yokoyama (Yokoyama, 2002, 2004). The density structure stands in contrast to that of Asama.

CONCLUSIONS

To understand the explosions like those that occurred at Mt. Asama, one must know whether or not the pressurized stage exists just before the explosions. First we provided direct evidence that the original crater is covered by the dense lava mound which functions as a vent cap. Second, a link between the intermittent collapses of the crater floor and an underlying porous region can be strong evidence for the fall-back of fragmented volcanic materials from the plume into the conduit. The spatial extent of each density anomaly is about 100 to 200 m. Cosmic-ray muon radiography provides a simple interpretation for various surface phenomena.

We anticipate our technique to be a starting point for more direct *in situ* monitoring of volcanic activities. For example, applied to multiple detectors distributed at different azimuths along the flanks of a volcanic cone, the radiographic method presented here could potentially provide three-dimensional images of volcanic density structure with a spatial resolution of about 30 to 60 m. Furthermore, with real-time readings, the method may help in predicting eruption by providing detailed images of volcanic density structure in a simple and straightforward manner. Further research is required to improve the ability to detect, attribute and understand volcanic activities, to reduce uncertainties and to predict a future eruption.

ACKNOWLEDGMENTS

The authors are deeply indebted to K. Kodama of Aichi University of Education and M. Komatsu of Nagoya University for their valuable contributions. Special funding arrangements by S. Okubo and related people of ERI and JSPS (Japanese Society of Promotion of Science) are acknowledged. H. Watanabe and T. Koyaguchi of ERI, K. Nagamine of UCR, I. Yokoyama M.J.A., H. Taira, and A. Yamada are also acknowledged for their valuable contributions. This work greatly benefited from reviews by B. Chouet and an anonymous reviewer.

References

Adair, R. K., and Kasha, H., 1976, Muon Physics, *in* Hughes, V. W., and Wu, C. S., editors, Muon Physics, volume 1: New York, Academic Press, p. 323.

Agostinelli, S., Allison, J., Amako, K., Apostolakis, J., Araújo, H. M., Arce, P., Asai, M., Axen, D. A., Banerjee, S., Barrand, G., Behner, F., Bellagamba, L., Boudreau, J., Broglia, L., Brunengo, A., Chauvie, S., Chuma, J., Chytracek, R., Cooperman, G., Cosmo, G., Degtyarenko, P. V., Dell'Acqua, A., De Paola, G. O., Dietrich, D. D., Enami, R., Feliciello, A., Ferguson, C., Fesefeldt, H. S., Folger, G., Foppiano, F., Forti, A. C., Garelli, S., Giani, S., Giannitrapani, R., Gibin, D., Gómez-Cadenas, J. J., González, I., Gracía-Abríl, G., Greeniaus, L. G., Greiner, W., Grichine, V. M., Grossheim, A., Gumplinger, P., Hamatsu, R., Hashimoto, K., Hasui, H., Heikkinen, A. M., Howard, A., Hutton, A. M., Ivanchenko, V. N., Johnson, A., Jones, F. W., Kallenbach, J., Kanaya, N., Kawabata, M., Kawabata, Y., Kawaguti, M., Kelner, S., Kent, P., Kodama, T., Kokoulin, R. P., Kossov, M., Kurashige, H., Lamanna, E., Lampen, T., Lara, V., Lefébure, V., Lei, F., Liendl, M., Lockman, W., Longo, F., Magni, S., Maire, M., Mecking, B. A., Medernach, E., Minamimoto, K., Mora De Freitas, P., Morita, Y., Murakami, K., Nagamatu, M., Nartallo, R., Nieminen, P., Nishimura, T., Ohtsubo, K., Okamura, M., O'Neale, S. W., O'Ohata, Y., Perl, J., Pfeiffer, A., Pia, M. G., Ranjard, F., Rybin, A., Sadilov, S., Di Salvo, E., Santin, G., Sasaki, T., Savvas, N., Sawada, Y., Scherer, S., Sei, S., Sirotenko, V. I., Smith, D., Starkov, N., Stöcker, H., Sulkimo, J., Takahata, M., Tanaka, S., Chernyaev, E., Safai-Tehrani, F., Tropeano, M., Truscott, P. R., Uno, H., Urbàn, L., Urban, P., Verderi, M., Walkden, A., Wander, W., Weber, H., Wellisch, J. P., Wenaus, T., Williams, D. C., Wright, D., Yamada, T., Yoshida, H., and Zschiesche, D., 2003, Geant4: A simulation tool kit: Nuclear Instruments and Methods in Physics Research Section A, v. 506 p. 250–303.

Alvarez, L. W., 1970, Search for Hidden Chambers in the Pyramids: Science, v. 167, p. 832–839, doi: 10.1126/science.167.3919.832.

Groom, D. E., Mokhov, N. V., and Striganov, S. I., 2001, Muon Stopping Power and Range Tables 10MeV–100 TeV: Atomic Data and Nuclear Data Tables, v. 78, p. 183–356, doi:10.1006/adnd.2001.0861.

Nakamura, T., Ariga, A., Ban, T., Fukuda, T., Fukuda, T., Fujioka, T., Furukawa, T., Hamada, K., Hayashi, H., Hiramatsu, S., Hoshino, K., Kawada, J., Koike, N., Komatsu, M., Matsuoka, H., Miyamoto, S., Miyanishi, K., Miyanishi, M., Morishima, K., Nada, H., Naganawa, N., Nakano, T., Narita, K., Natsume, M., Niwa, K., Nonaka, N., Park, B. D., Sato, O., Takahashi, S., Toshito, T., Uetake, T., Nakamura, M., Kuwabara, K., Nishiyama, S., Nonoyama, Y., and Kodama, K., 2006, The OPERA film: New nuclear emulsion for large-scale, high-precision experiments: Nuclear Instruments and Methods in Physics Research Section A, v. 556, p. 80–86.

Particle Data Group, 1998, Review of Particle Physics: The European Physical Journal C, v. 3, p. 1–794, doi:10.1007/s10052-998-0104-x.

Tanaka, H., Nagamine, K., Kawamura, N., Nakamura, S. N., Ishida, K., and Shimomura, K., 2003, Development of a two-fold segmented detection system for near horizontally cosmic-ray muons to probe the internal structure of a volcano: Nuclear Instruments and Methods in Physics Research Section A, v. 507, p. 657–669.

Tanaka, H. K. M., Nagamine, K., Nakamura, S. N. and Ishida, K., 2005, Radiographic measurements of the internal structure of Mt. West Iwate with near-horizontal cosmic-ray muons and future developments: Nuclear Instruments and Methods in Physics Research Section A, v. 555, p. 164–172.

Tanaka, H. K. M., Nakano, T., Takahashi, S., and Niwa, K., 2007, Development of an emulsion imaging system for cosmic-ray muon radiography to explore the internal structure of a volcano, Mt. Asama: Nuclear Instruments and Methods in Physics Research Section A, v. 575, p. 489–497.

Thompson, M. G., and Whalley, M. R., 1975, The production spectra of the parents of vertical cosmic ray muons: Journal of Physics G: Nuclear Physics, v. 1, p. L48-L50, doi: 10.1088/0305-4616/1/6/004.

Urabe, B., Watanabe, N., and Murakami, M., 2006, Topographic Change of the Summit Crater of Asama Volcano during the 2004 Eruption Derived from Airborne Synthetic Aperture Radar (SAR)Measurements: Bulletin of Geographical Survey Institute, v. 53, p. 1–6.

Yokoyama, I., 2002, Growth mechanism of the 1944 lava dome of Usu volcano in Hokkaido, Japan: Proceedings of the Japan Academy, Series B: Physical and Biological Sciences, v. 78, p. 6–11, doi:10.2183/pjab.78.6.

——— 2004, Formation processes of the 1909 Tarumai and the 1944 Usu lava domes in Hokkaido Japan: Annals of Geophysics, v. 47, p. 1811–1825, http://hdl.handle.net/2122/873.